Calculation of the Photoelectric Emission from Tungsten, Tantalum, and Molybdenum*

Irene Petroff and C. R. Viswanathan

*Electrical Sciences and Engineering Department, School of Engineering and Applied Science,
University of California, Los Angeles, California 90024*

(Received 20 August 1970)

A calculation of the photoelectric emission due to direct transitions between volume states of the crystal is carried out for tungsten, tantalum, and molybdenum. The calculations include a determination of the energy band structure by the augmented-plane-wave method for each metal. The Fermi energies and density-of-states histograms are obtained. The matrix elements for direct interband transitions are calculated throughout the Brillouin zone, and are found to vary widely as a function of k. The resulting histograms for the photoelectric yield and typical energy-distribution curves are presented.

I. INTRODUCTION

In recent years, the relationship between the band structure of solids and photoemission began to be appreciated as a means to correlate theoretical calculations with experimental results.[1-6] In the present investigation, the energy band structures of tungsten, tantalum, and molybdenum are calculated over an energy range which extends into the higher energy states from which the electrons seen in photoemission originate. Photoemission-yield histograms are obtained on the basis of the direct-transition model, and the dipole-transition matrix elements are calculated and included in the analysis. This is compared to the photoemission yield obtained by considering the optical-transition matrix elements to be constant.

The augmented-plane-wave (APW) calculation of the band structure is briefly discussed and the results presented in Sec. II. Section III deals with the calculation of the density of states. In Sec. IV working expressions for the optical-transition matrix elements are obtained by carrying out the integrations, and in Sec. V the photoemission-yield and energy-distribution curves are calculated. Section VI contains a discussion of the results obtained and a comparison with experiment when feasible.

II. BAND STRUCTURE

The band structure for the three materials investigated here is calculated by the APW method[7] as applied by Wood[8] to iron and by Mattheiss[9] to tungsten. The muffin-tin potential is constructed from the atomic orbitals of the single atom published by Herman and Skillman.[10] The contribution to the potential at a given lattice site from an atom on an adjacent site is found by Lowdin's α-summation method,[11] taking the spherically symmetric terms from the first- and second-nearest neighbors. The contributions to the Coulomb and exchange potentials are summed separately. The

full Slater exchange potential[12] is used. The lattice parameters are based on data given by Pearson[13] and are shown in Table I. The atomic configurations taken for the construction of the potential are the free-atom configurations: $(5d)^4 (6s)^2$ for tungsten, $(5d)^3 (6s)^2$ for tantalum, and $(4d)^5 (5s)^1$ for molybdenum.

The wave function $\Psi_k^{\alpha,l}$ is expanded in symmetrized augmented plane waves:

$$\Psi_k^{\alpha,l} = \sum_i \sum_j A_{ij}(\phi_i)_{ij}^{\alpha} , \tag{1}$$

$$(\phi_i)_{ij}^{\alpha} = (n_\alpha/G)\sum_R \Gamma^\alpha(R)_{ij} R\psi_i = \rho_{ij}^{\alpha} \psi_i . \tag{2}$$

The functions ψ_i in Eq. (2) are augmented plane waves:

$$\psi_i = e^{i\vec{k}_i \cdot \vec{r}} , \qquad\qquad r > R_s$$

$$= \sum_{l=0}^{\infty} \sum_{m=-l}^{l} (2l+1)i^l \, \frac{j_l(\vec{k}_i R_s)}{U_l(R_s)} \, U_l(r) \, \frac{(l-|m|)!}{(l+|m|)!}$$

$$\times P_l^{|m|} \cos\theta \, P_l^{|m|} \cos\theta_{ki} e^{im(\Phi-\phi_{ki})}, \quad r < R_s \tag{3}$$

where $U_l(r)$ satisfies the radial equation

$$\frac{1}{r^2}\frac{d}{dr}\left(r^2\frac{dU_l(r)}{dr}\right)+\left(-\frac{l(l+1)}{r^2}+[E-V(r)]\right)U_l(r)=0. \tag{4}$$

TABLE I. Lattice parameters for tungsten, tantalum, and molybdenum.

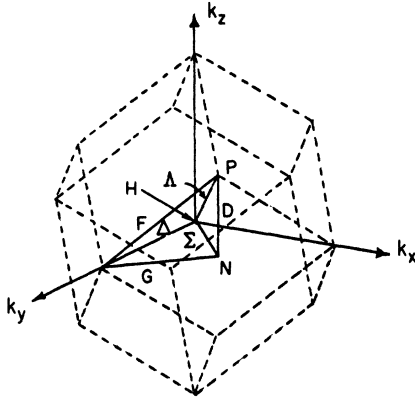| Material	Tungsten	Tantalum	Molybdenum
Structure type	bcc	bcc	bcc
First-neighbor distance in a.u.	5.17956	5.39674	5.14998
Second-neighbor distance in a.u.	5.98110	6.23177	5.94783
Slater-sphere radius in a.u.	2.58978	2.6987	2.57499
Atomic number	74	73	42

FIG. 1. Brillouin zone for body-centered cubic structure.

The symmetrized APW's of Eq. (2) are projected from the APW's by the projection operators corresponding to the group of the wave vector $\vec{k}$. In Eq. (1), the summation over i is over the different APW's ψ_i with vectors $\vec{k}+\vec{K}_i$, and the summation over j arises when more than one set of partners can be generated from one APW. The expansion coefficients A_{ij} are determined variationally[14] and are given by the solution of the system of equations

$$\sum_i \sum_j A_{ij} \langle (\phi_h)^\alpha_{lk} | H - E | (\phi_i)^\alpha_{lj} \rangle = 0, \quad h = 1, 2, 3, \ldots .$$

(5)

The individual terms in this system of equations can be simplified by applying standard relations of group representation. The coefficients of the A_{ij}'s become

$$(H - E)^\alpha_{(h,k),(i,j)} = (n_\alpha/G) \sum_R \Gamma_\alpha (R)^*_{kj} \langle \psi_h | H - E | \psi_i \rangle .$$

(6)

After replacing H by $-\nabla^2 + V(r)_{APW}$ and integrating, the expression that is obtained for $\langle \psi_h | H - E | R\psi_i \rangle$ is[15]

$$\langle \psi_h | H - E | R\psi_i \rangle = (\vec{k}_h \cdot R\vec{k}_i - E)$$

$$\times \left(\Omega\delta_{hi} - 4\pi R_s^2 \frac{j_i(|R\vec{k}_i - \vec{k}_h|R_s)}{|R\vec{k}_i - \vec{k}_h|} \right) + 4\pi R_s^2$$

$$\times \sum_{l=0}^{\infty} (2l+1) P_l \left(\frac{\vec{k}_h \cdot R\vec{k}_i}{|k_h| |k_i|} \right) j_l(k_h R_s) j_l(k_i R_s) \frac{U'_l(R_s)}{U_l(R_s)} .$$

(7)

In this expression $\vec{k}_h$ and $\vec{k}_i$ are members of the set $\vec{k} + \vec{K}_i$ where $\vec{K}_i$ is a reciprocal-lattice vector such that each vector $\vec{k}+\vec{K}_i$ cannot be obtained from a member of the set by an operation belonging to the group of $\vec{k}$. A solution for the A_{ij}'s will exist if the secular determinant of the system of Eqs. (5) is zero. The task of calculating the eigenvalues

of the crystal and thus obtaining the band structure consists in calculating the value of the determinant for a range of values of E. The eigenvalues will be those values of E for which that determinant is zero. The calculations have been carried out for 55 points in $\frac{1}{48}$ of the Brillouin zone. The points are distributed uniformly on a cubic mesh throughout the zone (Fig. 1). Each point is located at the corner of a cubic subzone having edge dimensions $\pi/4a$ with the edges being oriented parallel to the coordinate axes k_x, k_y, and k_z. There are 1024 points in the entire zone.

The band structures obtained by this method are tabulated in Tables II–IV for tungsten, tantalum, and molybdenum, respectively, and are graphed in Figs. 2–4. The zero of energy is taken at the constant potential between the Slater spheres. The eigenstates are labeled according to the notation of Bouckaert, Smoluchowski, and Wigner.[16] The general character of the band structure for each metal agrees with the pattern for bcc-iron transition metals as seen in Wood's calculation for bcc iron,[8] and Mattheiss's results for vanadium, chromium, and iron.[17] The similarity among the band structures for the three materials substantiates the validity of the rigid-band model for body-centered transition metals with comparable lattice constants. (However, this substantiation which is through band-structure calculations alone, is yet to be verified by experiment.) This is due to the nature of the APW calculation which is fairly insensitive to the depth of the muffin-tin potential, and depends only on the ratio $U'_1(R_s)/U_1(R_s)$ at the Slater-sphere radius. At that radius, the potential is very similar for all three materials. The heavier metals exhibit a stronger spin-orbit interaction than the lighter metals and this would, of course, impair the validity of the rigid-band model. In this investigation, however, this effect is not included. The results for tungsten are in very good agreement with Mattheiss's calculation[10] in the region where the two calculations have a common energy range. The present calculation includes higher s, p, and f bands in view of the photoemission calculation. If the energy difference $E(H_{25}) - E(H_{12})$ is considered to be a measure of the d bandwidth, the values obtained for W, Ta, and Mo are 0.77, 0.74, and 0.68 Ry, respectively.

III. DENSITY OF STATES

The density-of-states curves shown in Figs. 5–7 are based on a sample of 65 536 points in the full Brillouin zone. The additional points in the band structure are obtained by reducing the mesh by a factor of 4 by means of interpolation. The resulting number of points in the Brillouin zone at which energy eigenvalues are available increases from 1024 to 65 536. The interpolation is carried

TABLE II. Energy-band results for tungsten. The zero of energy coincides with the constant potential between the APW spheres, $V_{av} = -1.40432$ Ry.

$(a/\pi)k$	Band 1	Band 2	Band 3	Band 4	Band 5	Band 6	Band 7	Band 8	Band 9
Γ $(0,0,0)$	1 0.343	25' 0.748	25' 0.748	25' 0.748	12 0.959	12 0.959	25 1.914	25 1.914	25 1.914
Δ $(0,\frac{1}{4},0)$	1 0.368	5 0.747	5 0.747	2' 0.761	2 0.921	1 0.974	2 1.953	5 1.960	5 1.960
Δ $(0,\frac{1}{2},0)$	1 0.435	5 0.748	5 0.748	2' 0.796	2 0.830	1 1.013	2 2.043	5 2.084	5 2.084
Δ $(0,\frac{3}{4},0)$	1 0.519	2 0.719	5 0.763	5 0.763	2' 0.852	1 1.067	1 2.027	2 2.147	5 2.240
Δ $(0,1,0)$	1 0.572	2 0.612	5 0.806	5 0.806	2' 0.925	1 1.132	1 1.945	2 2.250	5 2.260
Δ $(0,\frac{5}{4},0)$	2 0.522	1 0.554	5 0.879	5 0.879	2' 1.007	1 1.226	1 2.015	5 2.093	5 2.093
Δ $(0,\frac{3}{2},0)$	2 0.455	1 0.486	5 0.982	5 0.982	2' 1.087	1 1.358	5 1.861	5 1.861	1 2.180
Δ $(0,\frac{7}{4},0)$	2 0.413	1 0.423	5 1.101	5 1.101	2' 1.148	1 1.499	5 1.656	5 1.656	1 2.320
H $(0,2,0)$	12 0.398	12 0.398	25' 1.170	25' 1.170	25' 1.170	15 1.556	15 1.556	15 1.556	1 2.280
Σ $(\frac{1}{4},\frac{1}{4},0)$	1 0.391	2 0.719	1 0.740	3' 0.800	4 0.962	4 1.951	2 2.003	1 2.019	+ 0.449
$(\frac{1}{4},\frac{1}{2},0)$	+ 0.449	− 0.701	+ 0.727	− 0.856	+ 0.873	+ 0.998	+ 1.992	+ 2.091	− 2.123
$(\frac{1}{4},\frac{3}{4},0)$	+ 0.515	+ 0.697	− 0.705	+ 0.833	− 0.924	+ 1.058	+ 1.962	+ 2.111	− 2.260
$(\frac{1}{4},1,0)$	+ 0.553	+ 0.631	− 0.739	+ 0.846	− 1.003	+ 1.141	+ 1.910	+ 2.159	− 2.262
$(\frac{1}{4},\frac{5}{4},0)$	+ 0.523	+ 0.574	− 0.804	+ 0.869	− 1.085	+ 1.261	+ 1.907	− 2.085	+ 2.125
$(\frac{1}{4},\frac{3}{2},0)$	+ 0.469	+ 0.505	− 0.899	+ 0.939	− 1.155	+ 1.424	+ 1.776	− 1.875	+ 2.240
G $(\frac{1}{4},\frac{7}{4},0)$	1 0.431	4 0.443	3 1.013	1 1.040	2 1.180	4 1.540	1 1.625	3 1.716	1 2.320
Σ $(\frac{1}{2},\frac{1}{2},0)$	1 0.474	2 0.657	1 0.730	1 0.928	3 0.941	4 0.977	4 1.925	1 2.074	2 2.230
$(\frac{1}{2},\frac{3}{4},0)$	+ 0.488	− 0.638	+ 0.752	+ 0.923	− 1.027	+ 1.029	+ 1.860	+ 2.012	− 2.240
$(\frac{1}{2},1,0)$	+ 0.497	− 0.657	+ 0.720	+ 0.912	− 1.115	+ 1.145	+ 1.832	+ 1.978	− 2.230
$(\frac{1}{2},\frac{5}{4},0)$	+ 0.499	+ 0.653	− 0.709	+ 0.869	− 1.182	+ 1.306	+ 1.787	+ 2.013	− 2.080
G $(\frac{1}{2},\frac{3}{2},0)$	1 0.489	4 0.570	3' 0.792	1 0.878	2 1.203	4 1.450	1 1.705	3 1.941	1 2.147
Σ $(\frac{3}{4},\frac{3}{4},0)$	1 0.460	2 0.605	1 0.857	1 0.976	4 1.007	3 1.129	4 1.771	1 1.899	3 2.320
$(\frac{3}{4},1,0)$	+ 0.453	− 0.603	+ 0.954	+ 0.961	+ 1.104	− 1.203	+ 1.747	+ 1.828	− 2.200
G $(\frac{3}{4},\frac{5}{4},0)$	1 0.469	3 0.639	4 0.763	1 0.903	2 1.227	4 1.249	1 1.756	1 1.862	3 2.120
N $(1,1,0)$	1 0.437	2 0.585	1' 0.997	1 0.979	4 1.024	3 1.235	4' 1.696	1 1.790	3' 2.200
Λ $(\frac{1}{4},\frac{1}{4},\frac{1}{4})$	1 0.413	3 0.711	3 0.711	2 0.842	3 0.943	3 0.943	2 1.965	3 2.039	3 2.039
$(\frac{1}{4},\frac{1}{2},\frac{1}{4})$	+ 0.467	+ 0.690	− 0.690	− 0.896	+ 0.911	+ 0.989	− 2.016	+ 2.045	− 2.126
$(\frac{1}{4},\frac{3}{4},\frac{1}{4})$	+ 0.524	− 0.693	+ 0.707	− 0.853	+ 0.991	+ 1.056	+ 1.947	− 2.145	+ 2.350

out in the wedge representing $\frac{1}{48}$ of the Brillouin zone, which contains the original 55 points for which the band structure was calculated. Values at the midpoints of the edges of the cubic subzones are obtained by linear interpolation. Values at the center of the cube faces are obtained by interpolation between previously obtained midpoints. Values at the cube centers are obtained by interpolating between previously obtained cube-face centers. At the wedge boundaries where the symmetry planes cut the cubic subzones along face or body diagonals, as in the case of the $NP\Gamma$, NPH, or ΓPH planes, reflection properties in the appropriate symmetry plane are used to complete the cubes in order to apply the interpolation scheme described.

In order to reduce the Brillouin zone mesh by a factor of 4, the interpolation procedure is applied twice. This results in 1785 points in $\frac{1}{48}$ of the Brillouin zone. Reflection properties are again applied to extend the results throughout the entire zone.

The density of states is plotted in units of electrons/atom/Ry. In each case the integral of the density of states is graphed in the same figure. The Fermi energy obtained from the integral of the density of states is 0.84195 Ry for tungsten, 0.70199 Ry for tantalum, and 0.80634 Ry for molybdenum. The density-of-states curve for tungsten is in good agreement with the corresponding results obtained by Mattheiss for this metal.[10]

TABLE II (Continued).

$(a/\pi)k$	Band 1	Band 2	Band 3	Band 4	Band 5	Band	Band 7	Band 8	Band 9
$(\frac{1}{4},1,\frac{1}{4})$	+ 0.563	− 0.606	+ 0.736	− 0.853	+ 1.033	+ 1.165	+ 1.876	− 2.109	+ 2.250
$(\frac{1}{4},\frac{5}{4},\frac{1}{4})$	− 0.543	+ 0.571	+ 0.748	− 0.905	+ 1.079	+ 1.319	+ 1.854	− 2.020	+ 2.179
$(\frac{1}{4},\frac{3}{2},\frac{1}{4})$	− 0.490	+ 0.538	+ 0.807	− 0.998	+ 1.122	+ 1.499	+ 1.761	− 1.827	− 2.320
F $(\frac{1}{4},\frac{7}{4},\frac{1}{4})$	3 0.455	3 0.455	1 0.910	3 1.111	3 1.111	3 1.636	3 1.636	1 1.663	3 2.360
$(\frac{1}{2},\frac{1}{2},\frac{1}{4})$	+ 0.500	− 0.648	+ 0.688	+ 0.936	− 0.977	+ 1.004	− 1.957	+ 2.061	− 2.155
$(\frac{1}{2},\frac{3}{4},\frac{1}{4})$	0.513	0.634	0.723	0.927	1.024	1.109	1.880	2.000	2.260
$(\frac{1}{2},1,\frac{1}{4})$	0.520	0.629	0.733	0.916	1.069	1.238	1.818	1.967	2.230
$(\frac{1}{2},\frac{5}{4},\frac{1}{4})$	0.528	0.633	0.693	0.916	1.118	1.399	1.762	1.942	2.147
$(\frac{1}{2},\frac{3}{2},\frac{1}{4})$	+ 0.516	− 0.575	+ 0.716	+ 0.956	− 1.133	− 1.537	+ 1.689	+ 1.856	+ 2.200
$(\frac{3}{4},\frac{3}{4},\frac{1}{4})$	+ 0.486	− 0.601	+ 0.809	+ 0.973	− 1.010	+ 1.203	− 1.798	+ 1.882	+ 2.225
$(\frac{3}{4},1,\frac{1}{4})$	0.479	0.603	0.832	0.969	1.065	1.296	1.760	1.816	2.163
$(\frac{3}{4},\frac{5}{4},\frac{1}{4})$	+ 0.493	+ 0.625	− 0.753	+ 0.930	− 1.123	− 1.387	+ 1.731	+ 1.852	+ 2.115
D $(1,1,\frac{1}{4})$	1 0.463	4 0.584	3 0.915	1 0.987	2 1.026	3 1.311	4 1.724	1 1.763	1 2.142
Λ $(\frac{1}{2},\frac{1}{2},\frac{1}{2})$	1 0.561	3 0.631	3 0.631	3 0.971	3 0.971	1 1.114	3 2.003	3 2.003	2 2.115
$(\frac{1}{2},\frac{3}{4},\frac{1}{2})$	+ 0.558	− 0.618	+ 0.676	− 0.955	+ 1.016	+ 1.225	+ 1.886	− 1.961	+ 2.142
$(\frac{1}{2},1,\frac{1}{2})$	+ 0.546	− 0.610	+ 0.721	− 0.946	+ 1.044	+ 1.348	+ 1.783	− 1.910	+ 2.114
$(\frac{1}{2},\frac{5}{4},\frac{1}{2})$	+ 0.569	− 0.602	+ 0.681	− 0.968	+ 1.057	+ 1.502	+ 1.709	− 1.827	+ 2.201
F $(\frac{1}{2},\frac{3}{2},\frac{1}{2})$	3 0.588	3 0.588	1 0.632	3 1.033	3 1.033	1 1.674	3 1.693	3 1.693	3 2.280
$(\frac{3}{4},\frac{3}{4},\frac{1}{2})$	+ 0.555	− 0.599	+ 0.724	+ 0.990	− 1.015	+ 1.337	+ 1.846	− 1.850	− 2.029
$(\frac{3}{4},1,\frac{1}{2})$	0.538	0.606	0.767	0.992	1.042	1.425	1.733	1.818	2.023
$(\frac{3}{4},\frac{5}{4},\frac{1}{2})$	+ 0.541	− 0.621	− 0.723	+ 0.981	− 1.050	− 1.513	+ 1.681	+ 1.784	+ 2.109
D $(1,1,\frac{1}{2})$	1 0.532	4 0.589	3 0.810	1 1.005	2 1.031	3 1.450	1 1.702	4 1.785	1 1.983
Λ $(\frac{3}{4},\frac{3}{4},\frac{3}{4})$	1 0.607	3 0.607	1 0.682	3 1.017	3 1.017*	1 1.450	1 1.808	3 1.848	3 1.848
$(\frac{3}{4},1,\frac{3}{4})$	+ 0.577	− 0.634	+ 0.711	− 1.016	+ 1.032	+ 1.537	+ 1.692	− 1.772	+ 1.904
F $(\frac{3}{4},\frac{5}{4},\frac{3}{4})$	1 0.556	3 0.677	3 0.677	3 1.021	3 1.021	1 1.654	3 1.658	3 1.658	1 2.029
D $(1,1,\frac{3}{4})$	4 0.608	1 0.612	3 0.718	1 1.026	2 1.034	3 1.596	1 1.652	4 1.802	1 1.810
P $(1,1,1)$	4 0.649	4 0.649	4 0.649	3 1.034	3 1.034	1 1.641	4 1.725	4 1.725	4 1.725

The calculation by Mattheiss extends to 1.3 Ry on the energy scale. The density of states at the Fermi energy can be used to calculate the low-temperature electronic specific-heat coefficient. The calculated and experimental values are compared in Table V. Loucks has found[20] that relativistic corrections lower the density of states at the Fermi level and that the ratio of γ(expt) to γ(APW) for molybdenum and tungsten becomes comparable when relativistic effects are taken into account in tungsten.

IV. ELECTRIC-DIPOLE TRANSITIONS

The transition matrix element M_{nm} for direct interband transitions is[21]

$$|M_{nm}|^2 = \frac{n\hbar e^2 V}{m^2 2\omega \epsilon_0 \Omega^2} \langle _\Omega\Psi_n | \vec{\epsilon} \cdot \vec{P} | \Psi_m \rangle^2 . \tag{8}$$

This expression follows directly from the Fermi "Golden rule" when the appropriate interaction Hamiltonian is substituted and the electric-dipole approximation is applied. The eigenfunctions Ψ_n and Ψ_m are combinations of symmetrized APW's according to Eq. (1). The integral $\langle _\Omega\Psi_n | \vec{\epsilon} \cdot \vec{P} | \Psi_m \rangle$ can be written in terms of basic APW's:

$$\langle _\Omega\Psi_n (\vec{k}, \vec{r}) | \vec{\epsilon} \cdot \vec{P} | \Psi_m (\vec{k}, \vec{r}) \rangle = \frac{n_\alpha n_\beta}{G^2}$$

$$\times \sum_i \sum_j A_i^* B_j \sum_R \sum_S \Gamma_{i\rho_i}^\alpha (R) \Gamma_{v\rho_j}^{\beta *} (S) \langle R\psi_i | \vec{\epsilon} \cdot \vec{P} | S\psi_j \rangle. \tag{9}$$

The integral $\langle R\psi_i | \vec{\epsilon} \cdot \vec{P} | S\psi_j \rangle$ can be evaluated by procedures similar to those used to obtain the elements $(H - E)_{(h,h')(i,j)}$ of Eq. (6). Outside the Slater sphere, where $\psi_i = e^{i\vec{k}_i \cdot \vec{r}}$, the range of integration is divided into an integration over the entire unit cell and an in-

TABLE III. Energy-band results for tantalum. The zero of energy coincides with the constant potential between the APW spheres, $V_{av} = -1.29352$ Ry.

$(a/\pi)k$	Band 1		Band 2		Band 3		Band 4		Band 5		Band 6		Band 7		Band 8		Band 9	
Γ (0,0,0)	1	0.298	25′	0.741	25′	0.741	25′	0.741	12	0.937	12	0.937	25	1.780	25	1.780	25	1.780
Δ (0,¼,0)	1	0.322	5	0.739	5	0.739	2′	0.753	2	0.900	1	0.952	2	1.820	5	1.823	5	1.823
Δ (0,½,0)	1	0.385	5	0.737	5	0.737	2′	0.786	2	0.811	1	0.990	2	1.917	5	1.940	5	1.940
Δ (0,¾,0)	1	0.468	2	0.704	5	0.750	5	0.750	2′	0.839	1	1.037	1	1.871	2	2.013	5	2.091
Δ (0,1,0)	1	0.531	2	0.602	5	0.787	5	0.787	2′	0.908	1	1.081	1	1.799	2	2.108	5	2.124
Δ (0,5/4,0)	2	0.517	1	0.531	5	0.854	5	0.854	2′	0.986	1	1.143	1	1.871	5	1.944	5	1.944
Δ (0,3/2,0)	2	0.453	1	0.477	5	0.952	5	0.952	2′	1.063	1	1.250	5	1.727	5	1.727	1	2.027
Δ (0,7/4,0)	2	0.414	1	0.423	5	1.068	5	1.068	2′	1.121	1	1.371	5	1.531	5	1.531	1	2.151
H (0,2,0)	12	0.400	12	0.400	25	1.142	25	1.142	25′	1.142	15	1.428	15	1.428	15	1.428	1	2.120
Σ (¼,¼,0)	1	0.343	2	0.712	1	0.730	3	0.789	1	0.905	4	0.940	4	1.816	2	1.864	1	1.883
(¼,½,0)	+	0.400	−	0.694	+	0.713	−	0.841	+	0.754	+	0.975	+	1.856	+	1.952	−	1.976
(¼,¾,0)	+	0.471	+	0.677	−	0.696	+	0.814	−	0.905	+	1.028	+	1.817	+	1.975	−	2.122
(¼,1,0)	+	0.522	+	0.611	−	0.727	+	0.824	−	0.980	+	1.089	+	1.768	+	2.019	−	2.122
(¼,5/4,0)	+	0.513	+	0.553	−	0.787	+	0.844	−	1.059	+	1.177	+	1.772	−	1.934	+	1.976
(¼,3/2,0)	+	0.460	+	0.490	−	0.876	+	0.907	−	1.126	+	1.310	+	1.649	−	1.737	+	2.064
G (¼,7/4,0)	1	0.430	4	0.441	3	0.984	1	1.005	2	1.152	4	1.415	1	1.506	3	1.557	1	2.191
Σ (½,½,0)	1	0.433	2	0.652	1	0.701	1	0.909	2	0.922	4	0.955	4	1.792	1	1.935	2	2.082
(½,¾,0)	+	0.461	−	0.633	+	0.710	+	0.900	−	0.990	+	1.002	+	1.727	+	1.875	−	2.100
(½,1,0)	+	0.479	−	0.651	+	0.685	+	0.886	−	0.087	+	1.091	+	1.700	+	1.845	−	2.098
(½,5/4,0)	+	0.488	+	0.628	−	0.698	+	0.844	−	1.153	+	1.221	+	1.663	+	1.877	−	1.924
G (½,3/2,0)	1	0.481	4	0.555	3	0.776	1	0.849	2	1.174	4	1.343	1	1.587	3	1.795	1	2.004
Σ (¾,¾,0)	1	0.443	2	0.602	1	0.791	1	0.952	4	0.985	3	1.101	4	1.643	1	1.766	3	2.190
(¾,1,0)	+	0.441	−	0.600	+	0.802	+	0.936	+	1.055	−	1.173	+	1.621	+	1.702	−	2.052
G (¾,5/4,0)	1	0.458	3	0.633	4	0.727	1	0.879	4	1.174	2	1.197	1	1.636	1	1.734	3	1.956
N (1,1,0)	1	0.427	2	0.583	1′	0.891	1	0.957	4	1.003	3	1.206	4′	1.571	1	1.669	3′	2.027
Λ (¼,¼,¼)	1	0.364	3	0.703	3	0.703	1	0.827	3	0.922	3	0.922	2	1.827	3	1.902	3	1.902
(¼,½,¼)	+	0.418	+	0.681	−	0.680	−	0.877	+	0.891	+	0.967	−	1.878	+	1.904	−	1.985
(¼,¾,¼)	+	0.481	−	0.677	+	0.691	−	0.836	+	0.967	+	1.025	+	1.804	−	2.001	+	2.230

tegration over the Slater sphere. The difference between the two integrals gives the required result. Taking $\vec{\epsilon} \cdot \vec{p} = p_x$, we have

$$\langle R\psi_i | p_x | S\psi_j \rangle$$

$$= \hbar(S\vec{k}_j)_x \left(\Omega \delta_{S\vec{k}_j, R\vec{k}_i} - 4\pi R_s^2 \frac{j_1(|S\vec{k}_j - R\vec{k}_i| R_s)}{|S\vec{k}_j - R\vec{k}_i|} \right). \tag{10}$$

Inside the Slater sphere, where ψ_i is expanded in spherical harmonics according to Eq. (3), direct differentiation to obtain $p_x S\psi_j$ results in expressions that do not simplify when integrated. As in the atomic case, the integral $\langle \Psi_n | p_x | \Psi_m \rangle_{sphere}$ can be transformed to a form which contains r rather than p as an operator.[22] Owing to the finite region of integration, the resulting expression contains surface terms. In terms of APW's, the transformed expression is

$$\langle \Psi_n | p_x | \Psi_m \rangle_{sphere} = \frac{n_\alpha n_\beta}{G^2} \sum_i \sum_j A_i^* B_j \sum_R \sum_S \Gamma_{lp_i}^\alpha (R)\, \Gamma_{vp_i}^{\beta*} (S)$$

TABLE III (Continued).

$(a/\pi)k$	Band 1	Band 2	Band 3	Band 4	Band 5	Band 6	Band 7	Band 8	Band 9
$(\frac{1}{4}, 1, \frac{1}{4})$	+ 0.530	− 0.594	+ 0.716	− 0.834	+ 1.008	+ 1.111	+ 1.738	− 1.973	+ 2.126
$(\frac{1}{4}, \frac{5}{4}, \frac{1}{4})$	− 0.535	+ 0.547	+ 0.731	− 0.881	+ 1.046	+ 1.239	+ 1.720	− 1.882	+ 2.021
$(\frac{1}{4}, \frac{3}{2}, \frac{1}{4})$	− 0.485	+ 0.524	+ 0.784	− 0.967	+ 1.088	+ 1.630	+ 1.630	− 1.698	− 2.195
F $(\frac{1}{4}, \frac{7}{4}, \frac{1}{4})$	3 0.452	3 0.452	1 0.881	3 1.078	3 1.078	3 1.515	3 1.515	1 1.539	3 2.250
$(\frac{1}{2}, \frac{1}{2}, \frac{1}{4})$	+ 0.456	− 0.643	+ 0.668	+ 0.916	− 0.955	+ 0.977	+ 1.923	− 1.822	− 2.004
$(\frac{1}{2}, \frac{3}{4}, \frac{1}{4})$	0.484	0.627	0.687	0.907	1.000	1.071	1.745	1.865	2.128
$(\frac{1}{2}, 1, \frac{1}{4})$	0.512	0.621	0.711	0.933	1.056	1.192	1.798	2.047	2.216
$(\frac{1}{2}, \frac{5}{4}, \frac{1}{4})$	0.514	0.613	0.676	0.892	1.082	1.322	1.634	1.811	1.988
$(\frac{1}{2}, \frac{3}{2}, \frac{1}{4})$	+ 0.507	− 0.560	+ 0.700	+ 0.927	− 1.099	− 1.436	+ 1.567	+ 1.724	+ 2.068
$(\frac{3}{4}, \frac{3}{4}, \frac{1}{4})$	+ 0.469	− 0.597	+ 0.753	+ 0.952	− 0.988	+ 1.161	− 1.669	+ 1.750	+ 2.077
$(\frac{3}{4}, 1, \frac{1}{4})$	0.466	0.598	0.781	0.946	1.034	1.245	1.632	1.689	1.997
$(\frac{3}{4}, \frac{5}{4}, \frac{1}{4})$	+ 0.481	+ 0.618	− 0.718	+ 0.906	− 1.085	− 1.311	+ 1.608	+ 1.726	+ 1.953
D $(1, 1, \frac{1}{4})$	1 0.451	4 0.581	3 0.846	1 0.965	2 1.006	3 1.262	4 1.599	1 1.640	1 1.976
Λ $(\frac{1}{2}, \frac{1}{2}, \frac{1}{2})$	1 0.510	3 0.623	3 0.623	3 0.951	3 0.951	1 1.075	3 1.868	3 1.868	2 1.965
$(\frac{1}{2}, \frac{3}{4}, \frac{1}{2})$	+ 0.531	− 0.606	+ 0.645	− 0.936	+ 0.994	+ 1.175	+ 1.751	− 1.831	+ 1.969
$(\frac{1}{2}, 1, \frac{1}{2})$	+ 0.531	− 0.595	+ 0.687	− 0.926	+ 1.018	+ 1.285	+ 1.650	− 1.786	+ 1.948
$(\frac{1}{2}, \frac{5}{4}, \frac{1}{2})$	+ 0.556	− 0.585	+ 0.658	− 0.944	+ 1.026	+ 1.448	+ 1.578	− 1.710	+ 2.035
F $(\frac{1}{2}, \frac{3}{2}, \frac{1}{2})$	3 0.572	3 0.572	1 0.618	3 1.004	3 1.004	1 1.546	3 1.585	3 1.585	3 2.171
$(\frac{3}{4}, \frac{3}{4}, \frac{1}{2})$	+ 0.535	− 0.591	+ 0.681	+ 0.970	+ 0.994	+ 1.276	+ 1.710	− 1.721	+ 1.874
$(\frac{3}{4}, 1, \frac{1}{2})$	0.523	0.595	0.725	0.970	1.018	1.602	1.695	1.870	2.250
$(\frac{3}{4}, \frac{5}{4}, \frac{1}{2})$	+ 0.529	+ 0.606	− 0.690	+ 0.959	− 1.023	− 1.437	+ 1.553	+ 1.669	+ 1.948
D $(1, 1, \frac{1}{2})$	1 0.516	4 0.582	3 0.763	1 0.984	2 1.010	3 1.375	1 1.574	4 1.659	1 1.837
Λ $(\frac{3}{4}, \frac{3}{4}, \frac{3}{4})$	3 0.595	3 0.595	1 0.640	3 0.997	3 0.997	1 1.378	1 1.651	3 1.725	3 1.725
$(\frac{3}{4}, \frac{3}{4}, \frac{3}{4})$	+ 0.565	− 0.615	+ 0.677	+ 0.996	+ 1.011	+ 1.451	+ 1.551	− 1.659	+ 1.766
F $(\frac{3}{4}, 1, \frac{3}{4})$	1 0.547	3 0.651	3 0.651	3 0.999	3 0.999	1 1.519	3 1.559	3 1.559	1 1.878
D $(1, 1, \frac{3}{4})$	4 0.595	1 0.592	3 0.686	1 1.005	2 1.014	3 1.504	1 1.513	4 1.682	1 1.685
P $(1, 1, 1)$	4 0.628	4 0.628	4 0.628	3 1.014	3 1.014	1 1.492	4 1.617	4 1.617	4 1.617

$$\times \frac{i}{2} \left((E_n - E_m) \langle R\psi_i | x | S\psi_j \rangle_{sphere} + \int_{R_s} \frac{\partial}{\partial r} (R\psi_i)^* \, x S\psi_j \, dS \right.$$

$$\left. - \int_{R_s} (R\psi_i)^* x \frac{\partial}{\partial r} S\psi_j \, dS - \int_{R_s} (R\psi_i)^* S\psi_j \frac{\partial x}{\partial r} dS \right) . \quad (11)$$

When integrated this expression becomes

$$\langle \Psi_n | p_x | \Psi_m \rangle_{sphere} = \frac{i}{2} \frac{n_\alpha n_\beta}{G^2} \sum_i \sum_j A_i^* B_j \sum_R \sum_S \Gamma_{l\rho_i}^\alpha (R) \, \Gamma_{\nu\rho_j}^{\beta*}(S)$$

$$\times i 4\pi \sum_{l=1}^\infty \sum_{m=1}^l [C_{l, l-1} P_{ij}(l-1)\cos ij + C_{l, l+1} P_{ij}(l+1)\cos ij$$

$$- C_{l+1, l} P_{ji}(l+1)\cos ji - C_{l-1, l} P_{ji}(l-1)\cos ji] , \quad (12)$$

where

TABLE IV. Energy-band results for molybdenum. The zero of energy coincides with the constant potential between the APW spheres, $V_{av} = -1.33993$ Ry.

$(a/\pi)k$	Band 1	Band 2	Band 3	Band 4	Band 5	Band 6	Band 7	Band 8	Band 9
$\Gamma\ (0,0,0)$	1 0.318	25′ 0.726	25′ 0.726	25′ 0.726	12 0.914	12 0.914	25 1.904	25 1.904	25 1.904
$\Delta\ (0,\frac{1}{4},0)$	1 0.342	5 0.724	5 0.724	2′ 0.738	2 0.883	2 0.927	2 1.928	5 1.946	5 1.946
$\Delta\ (0,\frac{1}{2},0)$	1 0.407	5 0.725	5 0.725	2′ 0.769	2 0.803	1 0.960	2 1.990	5 2.040	5 2.040
$\Delta\ (0,\frac{3}{4},0)$	1 0.490	2 0.703	5 0.738	5 0.738	2′ 0.818	1 1.006	1 1.970	2 2.100	5 2.200
$\Delta\ (0,1,0)$	1 0.546	2 0.605	5 0.775	5 0.775	2′ 0.882	1 1.068	1 1.920	2 2.210	5 2.220
$\Delta\ (0,\frac{5}{4},0)$	2 0.520	1 0.537	5 0.840	5 0.840	2′ 0.954	1 1.166	1 1.960	5 2.050	5 2.050
$\Delta\ (0,\frac{3}{2},0)$	2 0.457	1 0.481	5 0.932	5 0.932	2′ 1.022	1 1.315	5 1.771	5 1.771	1 2.120
$\Delta\ (0,\frac{7}{4},0)$	2 0.417	1 0.425	5 1.035	5 1.035	2′ 1.073	1 1.439	5 1.589	5 1.589	1 2.250
$H\ (0,2,0)$	12 0.403	12 0.403	25′ 1.091	25′ 1.091	25′ 1.091	15 1.505	15 1.505	15 1.505	1 2.230
$\Sigma\ (\frac{1}{4},\frac{1}{4},0)$	1 0.364	2 0.700	1 0.718	3 0.771	1 0.886	4 0.917	4 1.933	1 1.985	2 1.990
$(\frac{1}{4},\frac{1}{2},0)$	+ 0.422	− 0.683	+ 0.706	− 0.821	+ 0.839	+ 0.947	+ 1.957	+ 2.050	− 2.100
$(\frac{1}{4},\frac{3}{4},0)$	+ 0.490	+ 0.678	− 0.687	+ 0.802	− 0.880	+ 0.998	+ 1.931	+ 2.080	− 2.140
$(\frac{1}{4},1,0)$	+ 0.534	+ 0.616	− 0.717	+ 0.812	− 0.949	+ 1.076	+ 1.870	+ 2.120	− 2.245
$(\frac{1}{4},\frac{5}{4},0)$	+ 0.517	+ 0.558	− 0.775	+ 0.833	− 1.020	+ 1.196	+ 1.823	− 2.010	+ 2.050
$(\frac{1}{4},\frac{3}{2},0)$	+ 0.465	+ 0.495	− 0.860	+ 0.963	− 1.078	+ 1.350	+ 1.686	− 1.790	+ 2.160
$G\ (\frac{1}{4},\frac{7}{4},0)$	1 0.433	4 0.444	3 0.959	1 0.984	2 1.099	4 1.480	1 1.552	3 1.645	1 2.250
$\Sigma\ (\frac{1}{2},\frac{1}{2},0)$	1 0.453	2 0.644	1 0.704	1 0.865	3 0.895	4 0.920	4 1.892	1 2.040	2 2.150
$(\frac{1}{2},\frac{3}{4},0)$	+ 0.475	− 0.625	+ 0.721	+ 0.881	− 0.950	+ 0.973	+ 1.828	+ 1.914	− 2.140
$(\frac{1}{2},1,0)$	+ 0.488	− 0.643	+ 0.693	+ 0.871	− 1.044	+ 1.078	+ 1.774	+ 1.888	+ 2.130
$(\frac{1}{2},\frac{5}{4},0)$	+ 0.493	+ 0.632	− 0.689	+ 0.835	− 1.100	+ 1.237	+ 1.693	+ 1.936	− 2.000
$G\ (\frac{1}{2},\frac{3}{2},0)$	1 0.485	4 0.558	3 0.764	1 0.843	2 1.117	4 1.357	1 1.613	3 1.862	1 2.060
$\Sigma\ (\frac{3}{4},\frac{3}{4},0)$	1 0.453	2 0.596	1 0.816	1 0.926	4 0.954	3 1.056	4 1.748	1 1.794	3 2.220
$(\frac{3}{4},1,0)$	+ 0.448	− 0.595	+ 0.815	+ 0.914	+ 1.041	− 1.117	+ 1.698	+ 1.742	− 2.100
$G\ (\frac{3}{4},\frac{5}{4},0)$	1 0.465	3 0.627	4 0.732	1 0.866	2 1.136	4 1.177	1 1.656	1 1.810	3 2.050
$N\ (1,1,0)$	1 0.434	2 0.578	1′ 0.928	1 0.929	4 0.967	3 1.143	1 1.677	4′ 1.680	3′ 2.100
$\Lambda\ (\frac{1}{4},\frac{1}{4},\frac{1}{4})$	1 0.386	3 0.692	3 0.692	1 0.808	3 0.901	3 0.901	2 1.958	3 1.970	3 1.970
$(\frac{1}{4},\frac{1}{2},\frac{1}{4})$	+ 0.440	+ 0.673	− 0.673	− 0.859	+ 0.869	+ 0.939	− 1.980	+ 2.010	+ 2.090
$(\frac{1}{4},\frac{3}{4},\frac{1}{4})$	+ 0.500	− 0.676	+ 0.686	− 0.821	+ 0.939	+ 0.997	+ 1.908	− 2.100	+ 2.300
$(\frac{1}{4},1,\frac{1}{4})$	+ 0.543	− 0.596	+ 0.711	− 0.819	+ 0.976	+ 1.096	+ 1.830	− 2.070	+ 2.210
$(\frac{1}{4},\frac{5}{4},\frac{1}{4})$	− 0.538	+ 0.554	+ 0.724	− 0.865	+ 1.017	+ 1.245	+ 1.780	− 1.896	+ 2.050
$(\frac{1}{4},\frac{3}{2},\frac{1}{4})$	− 0.488	+ 0.529	+ 0.778	− 0.946	+ 1.053	+ 1.415	+ 1.684	− 1.726	− 2.220
$F\ (\frac{1}{4},\frac{7}{4},\frac{1}{4})$	3 0.455	3 0.455	1 0.869	3 1.043	3 1.043	3 1.560	3 1.560	1 1.593	3 2.290
$(\frac{1}{2},\frac{1}{2},\frac{1}{4})$	+ 0.477	− 0.636	+ 0.667	+ 0.893	− 0.929	+ 0.950	− 1.917	+ 2.020	− 2.110
$(\frac{1}{2},\frac{3}{4},\frac{1}{4})$	0.498	0.622	0.694	0.885	0.968	1.043	1.838	1.908	2.160
$(\frac{1}{2},1,\frac{1}{4})$	0.510	0.616	0.704	0.875	1.007	1.161	1.757	1.872	2.130
$(\frac{1}{2},\frac{5}{4},\frac{1}{4})$	0.519	0.616	0.673	0.876	1.049	1.329	1.680	1.838	2.030
$(\frac{1}{2},\frac{3}{2},\frac{1}{4})$	+ 0.510	− 0.563	+ 0.696	+ 0.910	− 1.061	− 1.448	+ 1.606	+ 1.760	+ 2.100
$(\frac{3}{4},\frac{3}{2},\frac{1}{4})$	+ 0.478	− 0.592	+ 0.770	+ 0.923	− 0.956	+ 1.124	− 1.768	+ 1.783	+ 2.125
$(\frac{3}{4},1,\frac{1}{4})$	0.473	0.593	0.793	0.921	1.003	1.216	1.688	1.752	2.100

TABLE IV (Continued).

$(a/\pi)k$	Band 1	Band 2	Band 3	Band 4	Band 5	Band 6	Band 7	Band 8	Band 9
$(\frac{3}{4},\frac{5}{4},\frac{1}{4})$	+ 0.487	+ 0.613	− 0.723	+ 0.885	− 1.052	− 1.298	+ 1.640	+ 1.785	+ 2.050
$D\ (1,1,\frac{1}{4})$	1 0.458	4 0.576	3 0.867	1 0.936	2 0.969	3 1.219	1 1.658	4 1.702	1 2.080
$\Lambda\ (\frac{1}{2},\frac{1}{2},\frac{1}{2})$	1 0.532	3 0.619	3 0.619	3 0.923	3 0.923	1 1.047	3 1.930	3 1.930	2 2.040
$(\frac{1}{2},\frac{3}{4},\frac{1}{2})$	+ 0.542	− 0.604	+ 0.650	− 0.909	+ 0.960	+ 1.145	+ 1.827	− 1.874	+ 2.060
$(\frac{1}{2},1,\frac{1}{2})$	+ 0.537	− 0.595	+ 0.691	− 0.902	+ 0.985	+ 1.272	+ 1.720	− 1.805	+ 2.030
$(\frac{1}{2},\frac{5}{4},\frac{1}{2})$	+ 0.559	− 0.587	+ 0.658	− 0.920	+ 0.996	+ 1.406	+ 1.645	− 1.712	+ 2.080
$F\ (\frac{1}{2},\frac{3}{2},\frac{1}{2})$	3 0.574	3 0.574	1 0.619	3 0.976	3 0.976	3 1.584	3 1.584	1 1.610	3 2.170
$(\frac{3}{4},\frac{3}{4},\frac{1}{2})$	+ 0.542	− 0.587	+ 0.691	+ 0.939	− 0.960	+ 1.246	+ 1.761	− 1.798	+ 1.955
$(\frac{3}{4},1,\frac{1}{2})$	0.528	0.592	0.732	0.940	0.983	1.349	1.658	1.747	1.980
$(\frac{3}{4},\frac{5}{4},\frac{1}{2})$	+ 0.533	+ 0.605	+ 0.694	+ 0.932	− 0.989	− 1.422	+ 1.606	+ 1.693	+ 2.000
$D\ (1,1,\frac{1}{2})$	1 1.521	4 0.578	3 0.770	1 0.951	2 0.972	3 1.351	1 1.617	4 1.741	1 1.901
$\Lambda\ (\frac{3}{4},\frac{3}{4},\frac{3}{4})$	3 0.592	3 0.592	1 0.652	3 0.961	3 0.961	1 1.351	1 1.758	3 1.767	3 1.767
$(\frac{3}{4},1,\frac{3}{4})$	+ 0.564	− 0.614	+ 0.680	− 0.961	+ 0.974	+ 1.444	+ 1.638	− 1.676	+ 1.837
$F\ (\frac{3}{4},\frac{5}{4},\frac{3}{4})$	1 0.547	3 0.652	3 0.652	3 0.964	3 0.964	3 1.556	3 1.556	1 1.598	1 1.963
$D\ (1,1,\frac{3}{4})$	4 0.592	1 0.593	3 0.687	1 0.969	2 0.975	3 1.498	1 1.588	4 1.726	1 1.729
$P\ (1,1,1)$	4 0.627	4 0.627	4 0.627	3 0.975	3 0.975	1 1.601	4 1.632	4 1.632	4 1.632

$$C_{l,\lambda}=j_l(\vec{k}_iR_s)\,j_\lambda(\vec{k}_jR_s)\left[(E_n-E_m)\frac{\int_0^{R_s}U_l(E_{n,r})\,U_\lambda(E_{m,r})\,r^3d^3r}{U_l(E_n,R_s)\,U_\lambda(E_m,R_s)}+\frac{U_l'(E_n,R_s)}{U_l(E_n,R_s)}R_s^3-\frac{U_\lambda'(E_m,R_s)}{U_\lambda(E_m,R_s)}R_s^3-R_s^2\right],$$

$$P_{ij}(l-1)=\frac{(l-m)!}{(l+m)!}\,(l+m-1)\,(l+m)\,P_l^m(\cos\theta_{R\vec{k}_i})\,P_{l+1}^{m-1}(\cos\theta_{S\vec{k}_j})\ ,$$

$$\cos ij=\cos[m\,(\phi_{R\vec{k}_i}-\phi_{S\vec{k}_j})+\phi_{S\vec{k}_j}]\ , \tag{13}$$

$$P_{ij}(l+1)=\frac{(l-m)!}{(l+m)!}\,[(l-m+2)\,(l-m+1)\,P_l^m(\cos\theta_{R\vec{k}_i})\,P_{l+1}^{m-1}(\cos\theta_{S\vec{k}_j})]\ .$$

The complete expression for the matrix-element integral can now be obtained by combining Eqs. (10) and (12):

$$\langle_\Omega\Psi_n|p_x|\Psi_m\rangle=\frac{n_\alpha n_\beta}{G^2}\sum_i\sum_j A_i^*B_j\sum_R\sum_S\Gamma_{lp_i}^\alpha(R)\,\Gamma_{vp_i}^{\beta*}(S)\left[(S\vec{k}_j)_x\left(\Omega\delta_{S\vec{k}_j,R\vec{k}_i}-4\pi R_s^2\,j_1\frac{(|S\vec{k}_j-R\vec{k}_i|R_s)}{|S\vec{k}_j-R\vec{k}_i|}\right)\right.$$

$$-2\pi\sum_{l=1}^\infty\sum_{m=1}^l[C_{l,l-1}\,P_{ij}(l-1)\cos ij+C_{l,l+1}\,P_{ij}(l+1)\cos ij$$

$$\left.-C_{l+1,l}\,P_{ji}(l+1)\cos ji-C_{l-1,l}\,P_{ji}(l-1)\cos ji]\right]\ . \tag{14}$$

Similar expressions are obtained for $\langle\Psi_n|p_y|\Psi_m\rangle$ and $\langle\Psi_n|p_z|\Psi_m\rangle$:

$$\langle\Psi_n|p_y|\Psi_m\rangle=\frac{n_\alpha n_\beta}{G^2}\sum_i\sum_j A_i^*B_j\sum_R\sum_S\Gamma_{lp_i}^\alpha(R)\,\Gamma_{vp_i}^\beta(S)$$

$$\times\left[(S\vec{k}_j)_y\left(\Omega\delta_{S\vec{k}_j,R\vec{k}_i}-4\pi R_s^2\frac{j_1(|S\vec{k}_j-R\vec{k}_i|R_s)}{|S\vec{k}_j-R\vec{k}_i|}\right)\right.$$

ENERGY (RYDBERGS)

$\Gamma \quad \Delta \quad H \quad G \quad N \quad \Sigma \quad \Gamma \quad \Lambda \quad P \quad D \quad N \quad D \quad P \quad F \quad H$
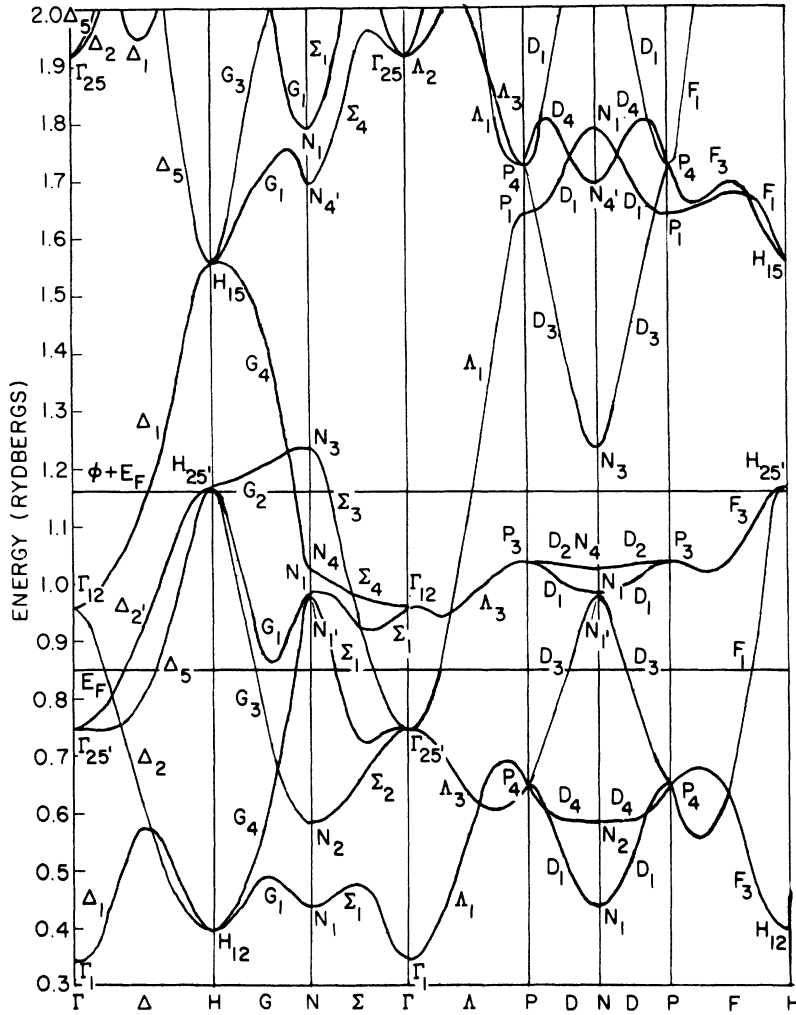
FIG. 2. Energy-band results along symmetry directions for tungsten.

$$-2\pi\sum_{l=1}^{\infty}\sum_{m=1}^{l}\left[C_{l,l-1}\,P_{ij}\,(l-1)\sin ij + C_{l,l+1}\,P_{ij}\,(l+1)\sin ij\right.$$

$$\left.-C_{l+1,l}\,P_{ji}\,(l+1)\sin ji - C_{l-1,l}\,P_{ji}\,(l-1)\sin ji\right]\;,\qquad(15)$$

$$\langle\Psi_n|p_\varepsilon|\Psi_m\rangle = \frac{n_\alpha n_\beta}{G^2}\sum_i\sum_j A_i^* B_j \sum_R\sum_S \Gamma_{lp_i}^{\alpha}(R)\,\Gamma_{vp_i}^{\beta*}(S)$$

$$\times\left[(S\vec{k}_j)_\varepsilon\left(\Omega\delta_{S\vec{k}_j,R\vec{k}_i} - 4\pi R_s^2\,\frac{j_i(|S\vec{k}_j - R\vec{k}_i|R_s)}{|S\vec{k}_j - R\vec{k}_i|}\right)\right.$$

$$-2\pi\sum_{l=0}^{\infty}\sum_{m=0}^{l}\frac{2(l-m+1)!}{(l+m)!}\cos m\,(\phi_{R\vec{k}_i} - \phi_{S\vec{k}_j})$$

$$\left.\times[C_{l,l+1}\,P_l^m\cos\theta_{R\vec{k}_i}\,P_{l+1}^m\cos\theta_{S\vec{k}_j} - C_{l+1,l}\,P_{l+1}^m\cos\theta_{R\vec{k}_i}\,P_l^m\cos\theta_{S\vec{k}_j}]\right]\;.\quad(16)$$

The expansion coefficients A_i and B_j are normalized according to the criterion $\langle{}_\Omega\Psi_k^{\alpha,\,l}|\Psi_k^{\alpha,\,l}\rangle = 1$. In terms of APW's and after some simplification,

the normalization condition becomes

$$\sum_i\sum_j A_i^* A_j a_{ij} = 1\;,\qquad(17)$$
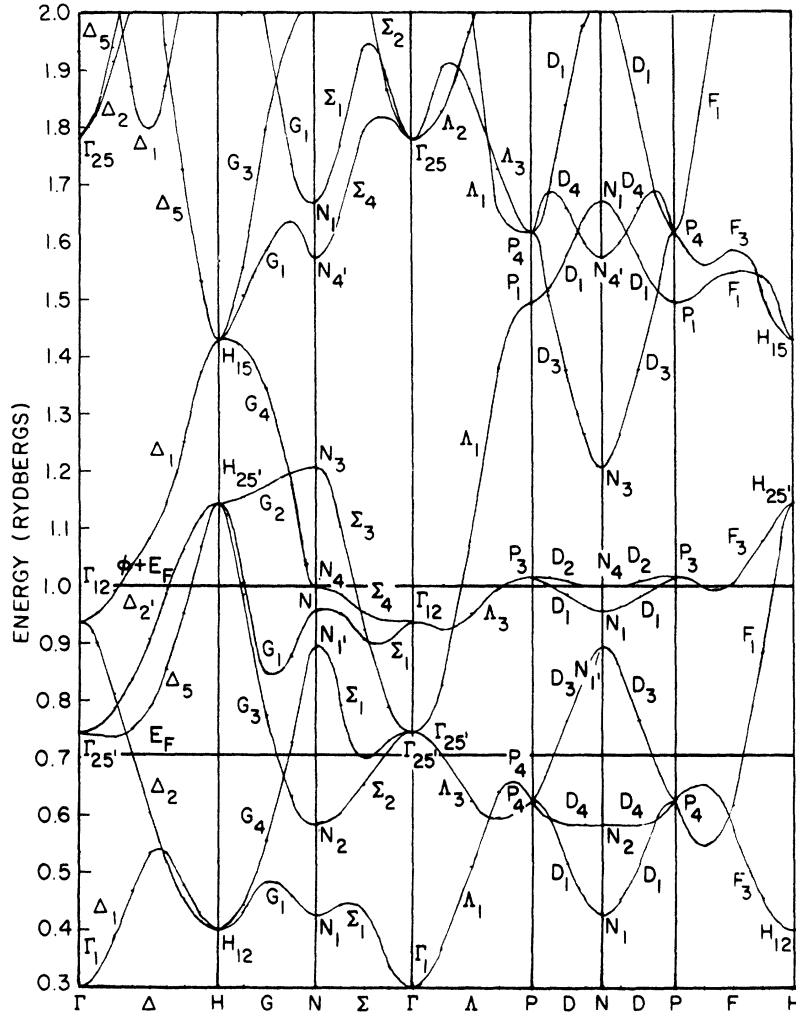
FIG. 3. Energy-band results along symmetry directions for tantalum.

where $a_{ij} = \langle \psi_i | \rho_{ij}^\alpha \psi_j \rangle$, and it can be shown that $a_{ij} = a_{ji}$. The complete expression for a_{ij} is thus

$$a_{ij} = \frac{n_\alpha}{G} \sum_R \Gamma_{\rho_i \rho_j}^{\alpha *} (R) \left[\Omega \delta_{R\vec{k}_i, \vec{k}_j} - 4\pi R_s^2 \frac{j_1 |R\vec{k}_j - \vec{k}_i | R_s)}{|R\vec{k}_j - \vec{k}_i|} \right.$$

$$+ 4\pi \sum_{l=0}^{\infty} \int_0^{R_s} r^2 U_l^2 (r) dr (2l + 1)$$

$$\left. \times \frac{j_l(\vec{k}_i R_s) j_l(\vec{k}_i R_s)}{u_l^2(R_s)} P_l \frac{\vec{k}_i \cdot R\vec{k}_j}{|k_i| |k_j|} \right] . \quad (18)$$

The unnormalized set of coefficients A_i is obtained by solving the system of Eq. (5). This means that all A_i's can be expressed in terms of A_1 as $A_i = A_1 c_i$, where the constant of proportionality is known. If the normalized coefficients are denoted by $\bar{A}_i$ as opposed to the unnormalized A_i, then we have

$$\bar{A}_1 = \left(\sum_{i=1}^{N} c_i^2 a_{ii} + 2 \sum_{i=2}^{N} \sum_{j=1}^{i-1} c_i c_j a_{ij} \right)^{-1/2} ,$$

$$\bar{A}_i = c_i \bar{A}_1 . \quad (19)$$

Owing to the high degree of symmetry of the bcc Brillouin zone in addition to the fact that the subsequent photoemission analysis is based on the assumption of a polycrystalline sample, the actual $|M_{fi}|^2$ is taken to be the average of

$$|M_{fi}|_x^2, \quad |M_{fi}|_y^2, \quad |M_{fi}|_z^2$$

corresponding to operators p_x, p_y, and p_z in the transition matrix element. Table VI shows relative values of $|M_{fi}|^2$ for transitions in the vicinity of the $N(1, 1, 0)$ point of the Brillouin zone. $|M(k)_{61}|^2$ corresponds to transitions between bands 6 and 1, and $|M(k)_{62}|^2$ corresponds to transitions between bands 6 and 2. The magnitude of the matrix elements is seen to vary greatly over this area. The
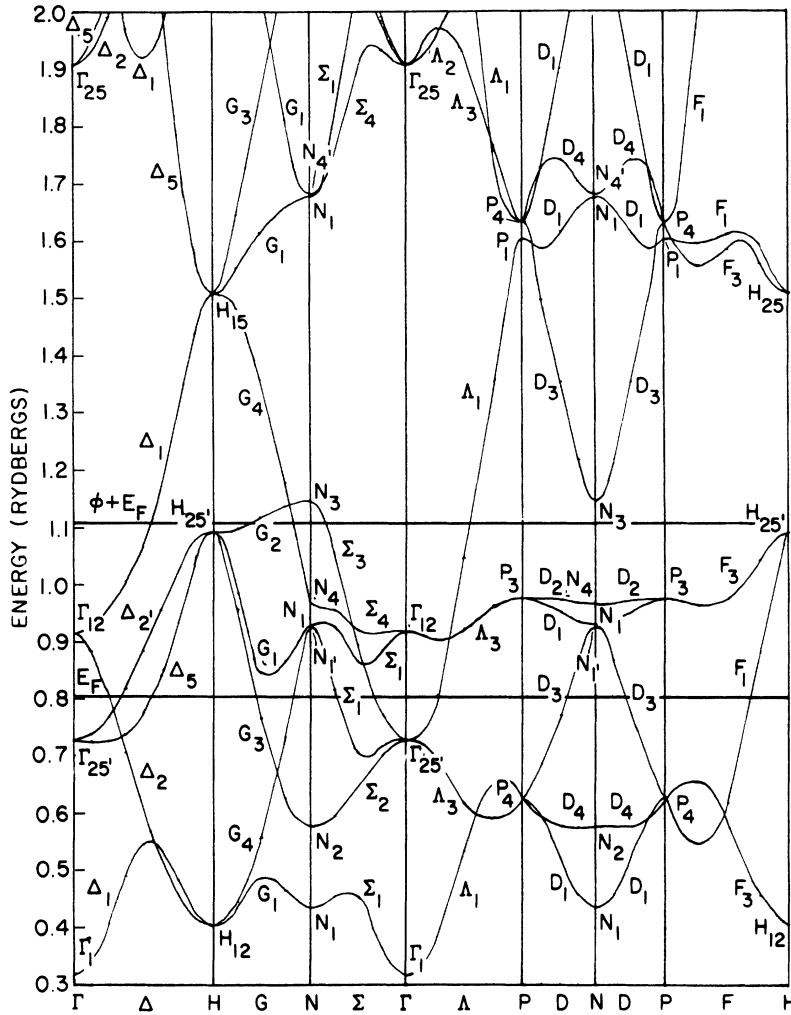
FIG. 4. Energy-band results along symmetry directions for molydbenum.

values of $|M(k)_{63}|^2$ in the vicinity of $P(1, 1, 1)$ are presented in Table VII. In this region the magnitude of the matrix elements is seen to be fairly constant. This justifies taking the matrix elements as constant, in some cases, when analyzing a given transition in the neighborhood of a specific point in the zone. However, in calculations such as photoemission yields where an integration over the entire zone is included, constant matrix elements are not justified.

V. PHOTOEMISSION

Photoemission is usually regarded as a three-step process: The first step is the photoexcitation of electrons into the higher states where the energy of the electrons is above the vacuum level; in the second step, the electrons move through the solid to the surface; and in the third step they escape into vacuum. The total photoexcitation rate is obtained by summing the individual transitions over all the states participating:

$$R(\hbar\omega) = \sum_{n,m} \frac{2V}{(2\pi)^3} \int_{\text{B.z.}} |M_{nm}|^2 \, \delta\left(E_n(\vec{k}) - E_m(\vec{k}) - \hbar\omega\right)$$

$$\times P_{Fm}(1 - P_{Fn}) d^3k \,, \tag{20}$$

where n and m are the band indices for the bands participating in the optical-excitation process, P_{Fm} and P_{Fn} are the corresponding Fermi factors, and a factor of 2 has been included because of spin degeneracy. Following Berglund and Spicer,[23] the transport and escape processes will be considered together. Assuming that the excited electrons are isotropically distributed in space and that electrons which scatter with significant energy loss do not escape, the rate of escape of electrons with energy between E and $E + dE$ is given by

$$n(E)\,dE = \frac{C(E)\,G_0(E)\,dE}{\alpha + 1/l} \,. \tag{21}$$

Here l is the mean free path for inelastic scattering and $C(E)$ is an escape function defined as fol-
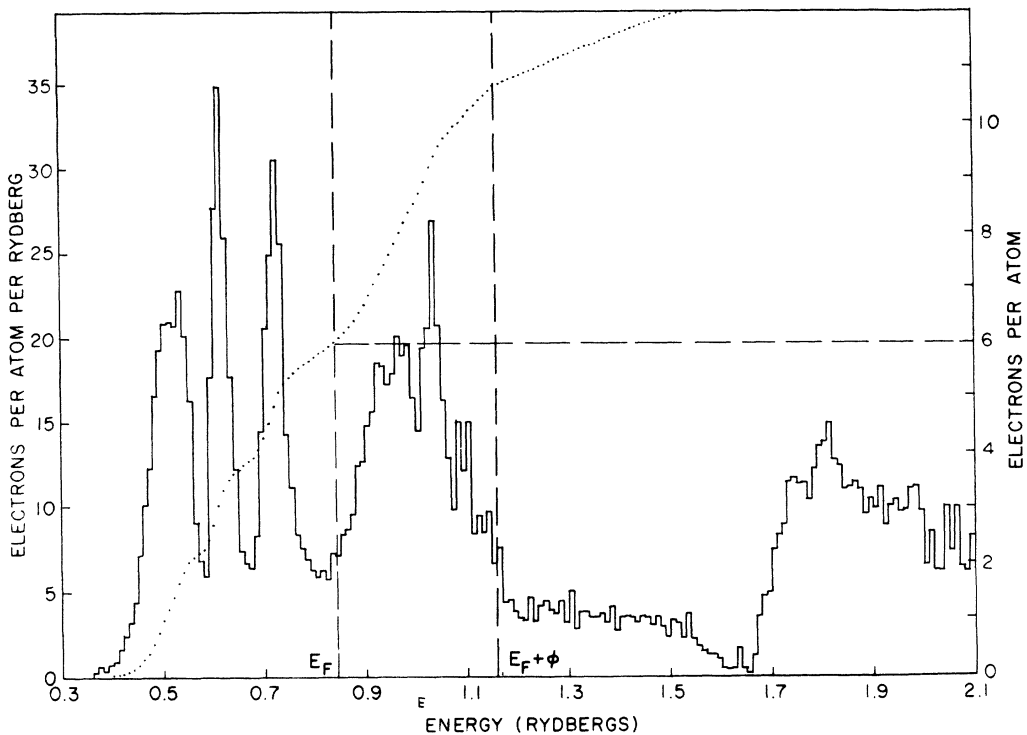
FIG. 5. Density-of-states curve for tungsten.

lows:

$$C(E) = \tfrac{1}{2}(1 - p_c/p) , \quad p \geq p_c$$

$$= 0 , \quad p < p_c \tag{22}$$

where p_c is the minimum component of momentum
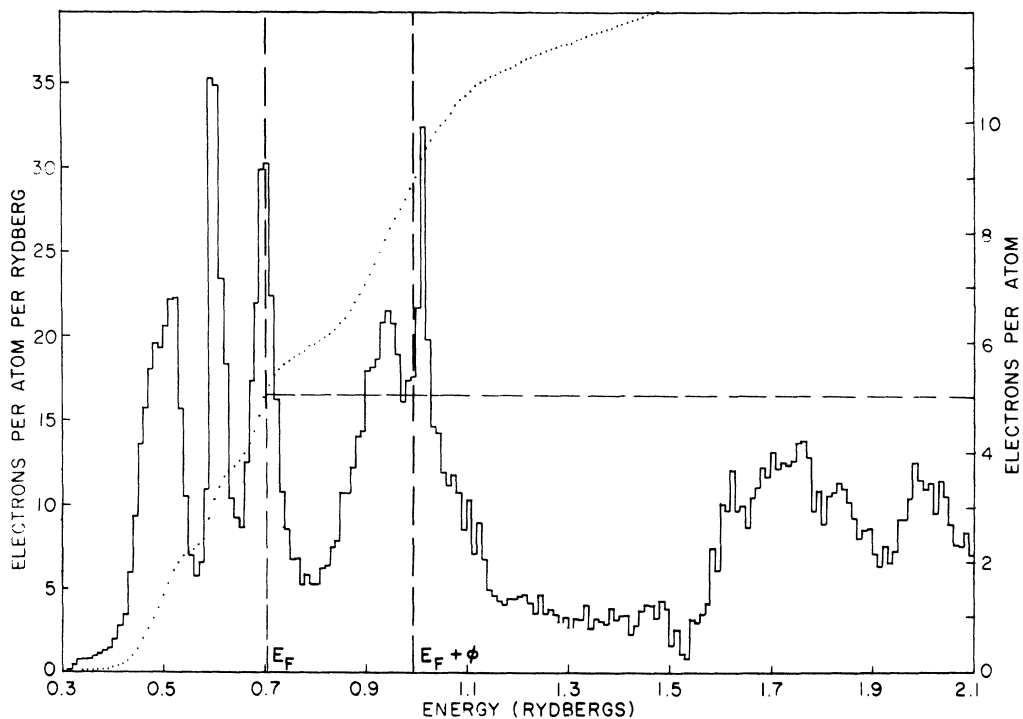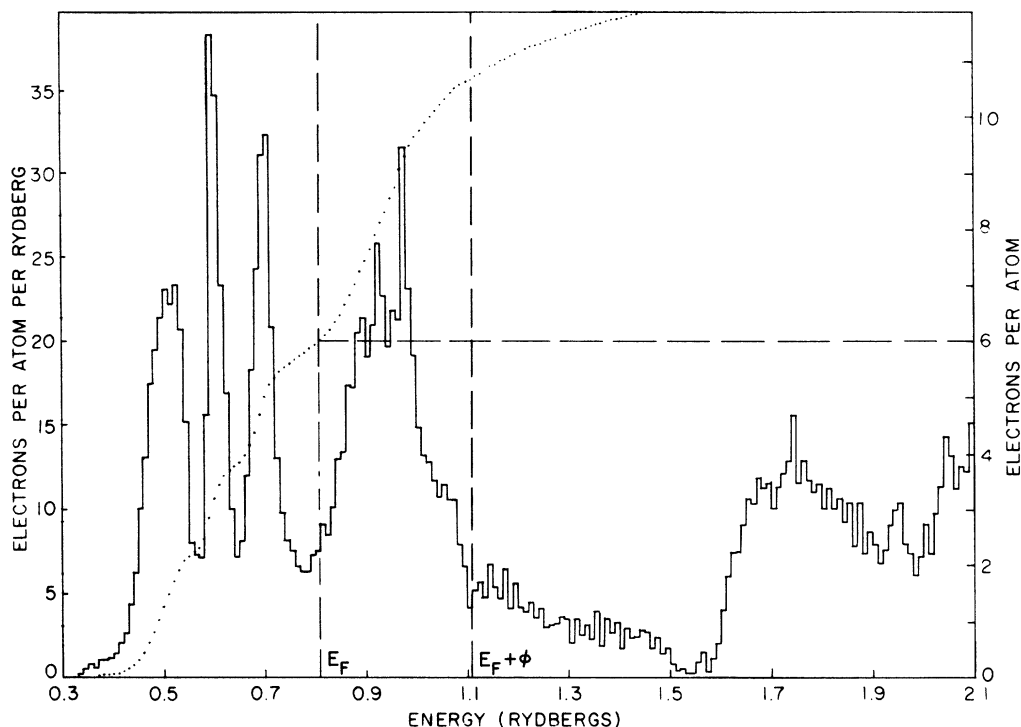

FIG. 6. Density-of-states curve for tantalum.

FIG. 7. Density-of-states curve for molybdenum.

perpendicular to the surface. A simple expression for p_c can be obtained if the energy of a given band n is approximated by

$$E_n(k) = E_n^0 + \frac{\hbar^2 |k|^2}{2m} \quad , \tag{23}$$

where E_n^0 is the lowest extremum of the band. In that case

$$p_c = [2m \, (E_{vac} - E_n^0)]^{1/2} \, , \quad E_n^0 \le E_{vac}$$

$$= 0 \, , \qquad\qquad\qquad E_n^0 > E_{vac} \tag{24}$$

$$p = \{2m \, [E_n(k) - E_n^0]\}^{1/2} \, .$$

The function $G_0(E)$, as defined by Berglund and Spicer, is the coefficient of the attenuation factor

TABLE V. Electronic specific heat (10^{-4}cal/mole $^\circ K^2$).

Value \ Material	Tungsten	Tantalum	Molybdenum
Calc.	3.1	12.1	3.54
Handbook Chem. Phys. (Ref. 18)	3.107	13.6	5.21
Hultgren et al. (Ref. 19)	2.5(±1.0)	13.5(±1.0)	5.26

$e^{-\alpha x}$ in the expression for the transition rate per unit area to energies between E and $E + dE$, in a slab of width dx, at a distance x from the surface on which the light is incident. We have

$$r''(\hbar\omega, E, x) \, dE \, dx = G_0(E) \, dE \, e^{-\alpha x} dx \, . \tag{25}$$

The total transition rate to energies between E and $E + dE$ is then

$$r'(\hbar\omega, E) \, dE = [G_0(e)/\alpha] \, dE \, . \tag{26}$$

The rate of escape for these electrons is given by Eq. (21). Thus the ratio $n(E) \, dE / r'(\hbar\omega, E) \, dE$ is

TABLE VI. Relative magnitude of $M\,(k)_{61}^2$ and $M(k)_{62}^2$ in the vicinity of $N(1,1,0)$ for tungsten.

k	$\mid M(k)_{61} \mid^2$	$\mid M(k)_{62} \mid^2$
$(\frac{3}{4}, \frac{3}{4}, 0)$	0.461×10^{-17}	0.627×10^{-4}
$(\frac{3}{4}, 1, 0)$	0.691×10^{-5}	0.282×10^{-4}
$(\frac{3}{4}, \frac{5}{4}, 0)$	0.188×10^{-4}	0.108×10^{-16}
$(1, 1, 0)$	0.545×10^{-16}	0.127×10^{-5}
$(\frac{3}{4}, \frac{3}{4}, \frac{1}{4})$	0.487×10^{-5}	0.427×10^{-4}
$(\frac{3}{4}, 1, \frac{1}{4})$	0.124	0.239×10^{-2}
$(\frac{3}{4}, \frac{5}{4}, \frac{1}{4})$	0.675	0.258
$(1, 1, \frac{1}{4})$	0.723×10^{-7}	0.706×10^{-7}

I. PETROFF AND C. R. VISWANATHAN

TABLE VII. Relative magnitude of $M(k)_{63}^2$ in the vicinity of $P(1,1,1)$ for tungsten.

k	$\lvert M(k)_{63}\rvert^2$
$(\frac{1}{2},\frac{1}{2},\frac{1}{2})$	0.331×10^{-2}
$(\frac{3}{4},\frac{3}{4},\frac{1}{2})$	0.371×10^{-2}
$(\frac{3}{4},\frac{3}{4},\frac{3}{4})$	0.769×10^{-2}
$(\frac{3}{4},1,\frac{3}{4})$	0.326×10^{-2}
$(1,1,\frac{3}{4})$	0.544×10^{-2}
$(1,1,1)$	0.000

equal to $\alpha C(E)/(\alpha+1/l)$ and

$$n(E)\,dE = \frac{\alpha C(E)}{\alpha+1/l}\, r'\,(\hbar\omega,E)\,dE \ . \qquad (27)$$

In this case, the transition rate is calculated on the basis of transition probabilities per unit volume. The transition rate per unit volume to energies between E and $E+dE$ is obtained from Eq. (20):

$$R'\,(\hbar\omega,E)\,dE = \sum_{n,m}\, [2V/(2\pi)^3]$$

$$\times \int_{\text{B.z.}}\, \lvert M_{nm}\rvert^2\,\delta\,[E_n\,(\vec{k})\,-E_m(\vec{k})-\hbar\omega]$$

$$\times P_{Fm}(1-P_{Fn})\,\delta\,[E-E_n\,(\vec{k})]\,d^3k\,dE \ . \qquad (28)$$

The rate of escape is obtained by utilizing Eq. (27). All yields are normalized to the total number of photons absorbed. With such a normalization, we have

$$N(E)\,dE = \frac{\alpha l}{\alpha l+1}\,\frac{\sum_{n,m}\int_{\text{B.z.}}C(E)\,(1-P_{Fn})\,P_{Fm}\lvert M_{nm}(\vec{k})\rvert^2\,x\delta\,[E-E_n\,(\vec{k})]\,\delta\,[E_n\,(\vec{k})-E_m(\vec{k})-\hbar\omega]\,d^3k\,dE}{\sum_{n,m}\int_{\text{B.z.}}\lvert M_{nm}(\vec{k})\rvert^2\,P_{Fm}(1-P_{Fn})\,\delta\,[E_n\,(\vec{k})-E_m(\vec{k})-\hbar\omega]\,d^3k} \ . \qquad (29)$$

The mean free path l for inelastic scattering will depend on the group velocity $v_g = (1/\hbar)\,\nabla_{\vec{k}}E$. In this analysis, however, the variation of l with $\vec{k}$ will not be considered. Furthermore, independently of the value taken for v_g, l will be a function of the energy of the excited electron. According to Krolikowski and Spicer,[3] l will vary from 40 to 15 Å for the range of energies of interest here, i.e., approximately 6–10 eV above the Fermi level. If α is taken as $5\times10^5\,\text{cm}^{-1}$, the factor $\alpha l/(\alpha l+1)$ will vary from 0.167 to 0.07. In view

of the approximation already made with respect to the variation of l with v_g, this factor will be assigned a constant value of 0.1. Such an approximation will affect the shape of the yield curve by emphasizing somewhat the contributions from high-energy final states and decreasing the contribution from low-energy final states. The character of the structure of the energy-distribution curves, however, is not affected by this factor.

The total yield as a function of photon energy is obtained by integrating $N(E)\,dE$:
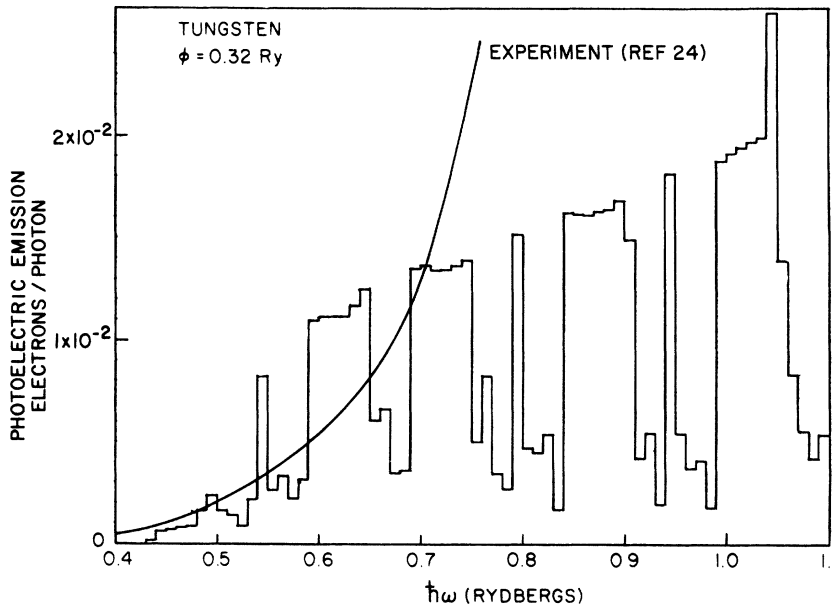

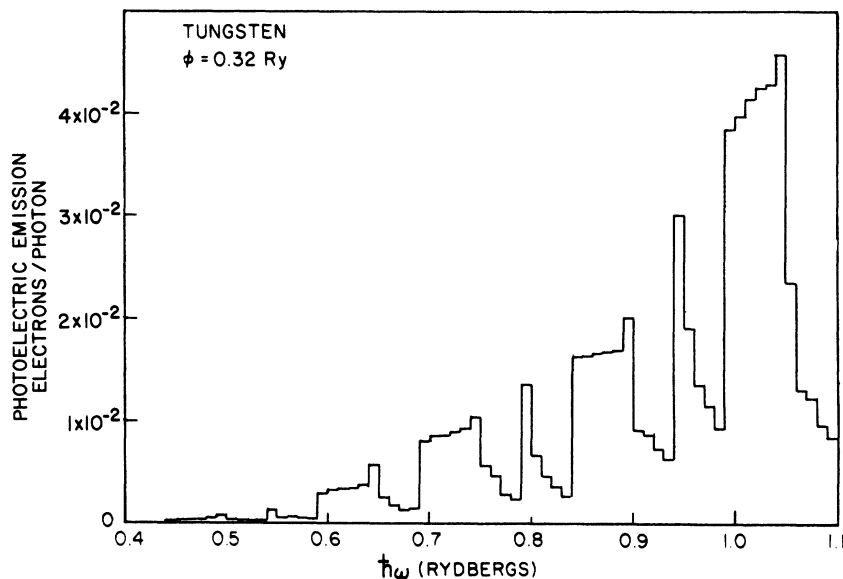FIG. 8. Photoelectric emission of tungsten, matrix elements included.

FIG. 9. Photoelectric emission of tungsten, constant matrix elements.

$$Y(\hbar\omega) = \frac{\alpha l}{\alpha l + 1} \frac{\sum_{n,m} \int_{B.z.} C_n(E)(1 - P_{Fn}) P_{Fm} |M_{nm}(\vec{k})|^2 x \delta [E_n(\vec{k}) - E_m(\vec{k}) - \hbar\omega] d^3k}{\sum_{n,m} \int_{B.z.} |M_{nm}(\vec{k})|^2 P_{Fm}(1 - P_{Fn}) \delta [E_n(\vec{k}) - E_m(\vec{k}) - \hbar\omega] d^3k} \tag{30}$$

The contribution of direct transitions to the photo-electric emission as a function of photon energy is plotted in Figs. 8–11. A comparison of Figs. 8 and 9 shows the effect of the transition matrix elements upon the photoelectric yield.

The tungsten and molybdenum yields are compared with reported experimental results, [24,25] as shown in Figs. 8 and 11. The experimental curve in Fig. 8 is a relative yield indicating the shape of the curve and should not be compared to the value of the cal-

culated yield. In Fig. 11 the calculated and experimental curves can be compared directly. The calculated yields are based on a reduced number of pair states, because many pair states are eliminated by the requirement that the final state lie above the work function, and that the transition be of the "direct" variety. This feature reduces the quality of the histogram obtained. The escape function $C_n(E)$ is different for each band n and would tend to accentuate discontinuities between
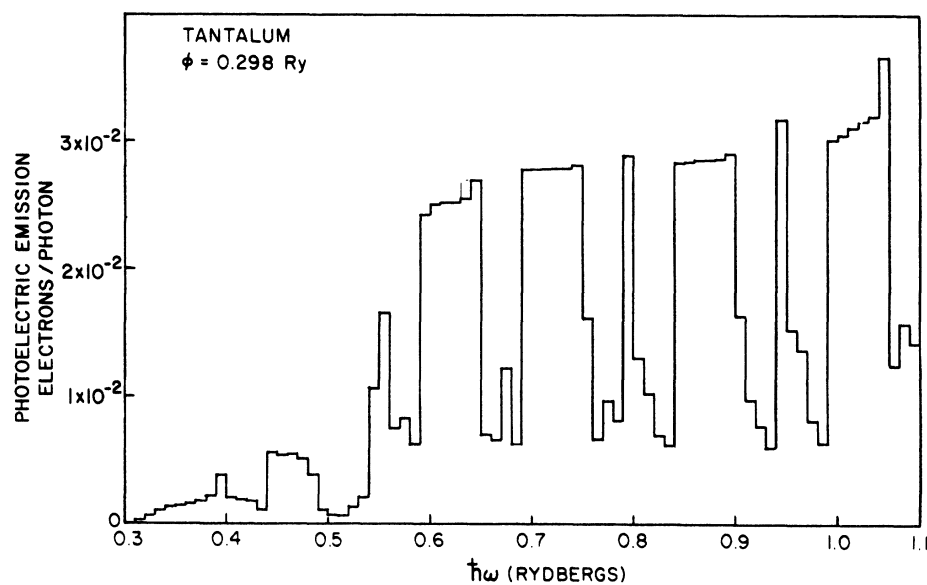
FIG. 10. Photoelectric emission of tantalum, matrix elements included.
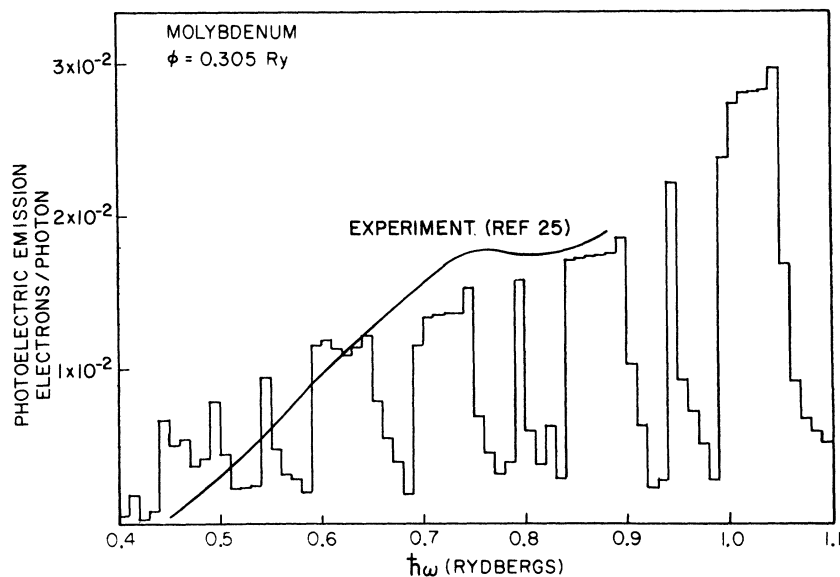
FIG. 11. Photoelectric emission of molybdenum, matrix elements included.

pair states where the energy separation is comparable but where the final states belong to different bands. These considerations would contribute to the saw-tooth appearance of the calculated yields, which is not apparent in the experimental curves.

The construction of the energy-distribution curves (EDC) requires a second sampling of the sample already obtained for the photoelectric-emission histogram. This is seen to arise from the second δ function in Eq. (29). As a result, the

number of points available after carrying out the double-interpolation procedure is no longer sufficient to provide a high-quality histogram. The points obtained by the interpolation procedure described in Sec. III were not interpolated further because the interpolation scheme used does not take into account the symmetry characteristics of each point of the Brillouin zone, which, in the case of the matrix elements, is of paramount importance.
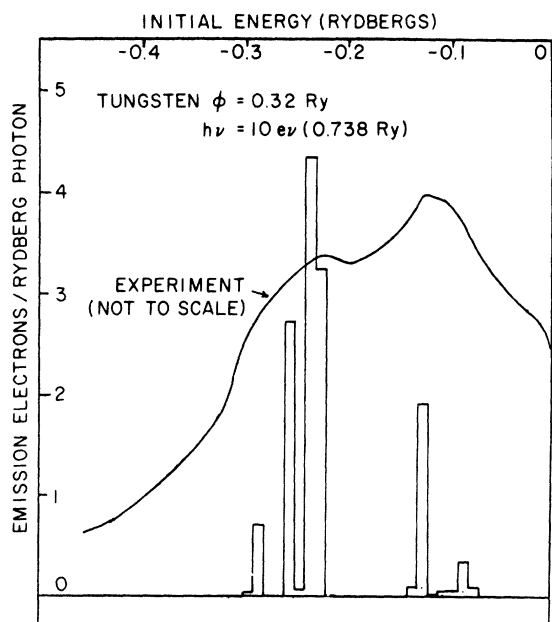
FIG. 12. Energy distribution of emitted electrons for tungsten, matrix elements included.
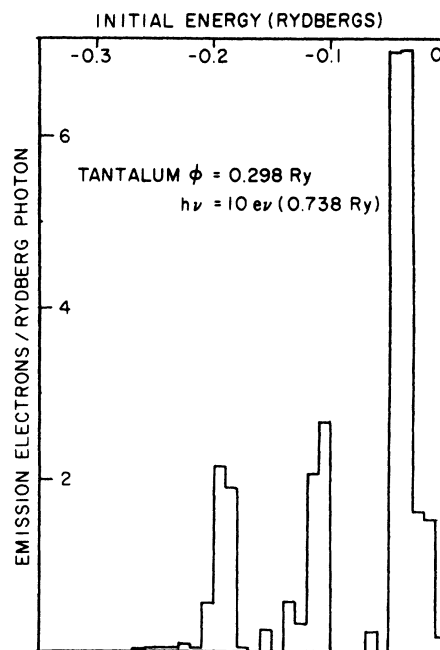
FIG. 13. Energy distribution of emitted electrons for tantalum, matrix elements included.
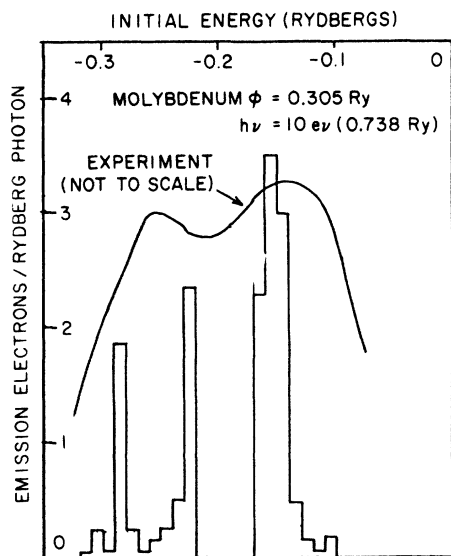
FIG. 14. Energy distribution of emitted electrons for molybdenum, matrix elements included.

Figures 12–14 show the EDC's for tungsten, tantalum, and molybdenum, respectively, at a photon frequency of 10 eV. The transitions involved include the $N_2 \leftrightarrow N_3$ transitions in the vicinity of the $N(1, 1, 0)$ point. The EDC's are plotted as a function of the energy of the initial state, with the Fermi level taken as reference. The work functions are taken from the *Handbook of Chemistry and Physics* (Ref. 18). The EDC's of tungsten and molybdenum were tentatively compared with reported experimental results[24,25] as shown in Figs. 12 and 14. The location of the main structure in the experimental curves appears to be correlated to the maxima in the theoretical direct-transition contributions to the photoemission. Owing to the poor quality of the energy-distribution histograms, a more detailed comparison between the experimental and theoretical curves could not be made.

Zeisse[24] has compared his 10.20-eV experimental EDC to the calculated density of states of Mattheiss[9] and has obtained a good agreement. If nondirect transitions constitute a sizable portion of the yield, the EDC can indeed be expected to reflect the density-of-states curve corresponding to the initial states, because, in this case, the final states correspond to the flat region in the density-

of-states curve, roughly between 1.2 and 1.6 Ry (see Fig. 5), and the emission is proportional to the product of the densities of initial and final states.

VI. CONCLUSION

The photoelectric-emission results show that, in the case of direct transitions, the inclusion of transition probabilities in the calculation has a significant effect upon the emission yield. The energy band structures for the three materials were calculated without correcting for the spin-orbit interaction. Although such corrections are negligible in the lighter elements such as molybdenum, their importance increases for the higher mass numbers. However, it is generally known that a variation of the Slater approximation for the exchange term in the crystal potential can cause modifications in the band structure which are of the same order of magnitude as those caused by spin-orbit corrections. The nonspherical terms in the crystal potential, thus far neglected, will also contribute to modifications in the band structure. The formulation of a more exact crystal potential would therefore be necessary to improve the accuracy of the corresponding band structure. The transport of excited electrons through the material and their escape probability are complex processes. A simplified analysis is applied to these phenomena in this study. A more accurate in-depth analysis would, of course, improve the accuracy of the calculated photoemission. However, the procedure used is sufficiently accurate for a first-order evaluation of the direct-transition contribution to the photoemission. Finally, it must be noted that a more sophisticated scheme of interpolation is required to improve the histograms resulting from the calculations. Some form of interpolation is necessary in view of the lengthy calculations required to obtain the eigenvalues and especially the dipole matrix elements at a given point in the Brillouin zone. The amount of computer time involved limits the number of points at which the eigenvalues and the corresponding transition matrix elements can be calculated.

[1]W. E. Spicer, in *Eighth International Conference on the Phenomena in Ionized Gases, Vienna*, 1968 (IAEA, Vienna, Austria, 1968), pp. 271–289.

[2]D. Brust, Phys. Rev. **139**, A489 (1965).

[3]W. F. Krolikowski and W. E. Spicer, Phys. Rev. **185**, 882 (1969).

[4]N. W. Smith and W. E. Spicer, Optics Commun. **1**, 157 (1969).

[5]J. F. Janak, D. E. Eastman, and A. R. Williams,

in *Proceedings of the Conference on Electronic Density of States* (Natl. Bur. Std., U. S. GPO, Washington, D. C., 1969).

[6]N. V. Smith, Phys. Rev. Letters **23**, 1452 (1969).

[7]J. C. Slater, Phys. Rev. **51**, 846 (1937).

[8]J. H. Wood, Phys. Rev. **126**, 517 (1962).

[9]L. F. Mattheiss, Phys. Rev. **139**, A1893 (1965).

[10]F. Herman and S. Skillman, *Atomic Structure Calculations* (Prentice-Hall, Englewood Cliffs, N. J., 1963).

[11]P. O. Lowdin, Advan. Phys. **5**, 1 (1956).

[12]J. C. Slater, Phys. Rev. **81**, 385 (1951).

[13]W. B. Pearson, *Handbook of Lattice Spacings and Structures of Metals and Alloys* (Pergamon, New York, 1958), Vol. I, pp. 85, 126, and 130.

[14]T. L. Loucks, *Augmented Plane Wave Method* (Benjamin, New York, 1967), pp. 24–32.

[15]J. C. Slater, *Quantum Theory of Molecules and Solids* (McGraw-Hill, New York, 1965), Vol. 2, pp. 461–465.

[16]L. P. Bouckaert, R. Smoluchowski, and E. Wigner, Phys. Rev. **50**, (1936).

[17]L. F. Mattheiss, Phys. Rev. **134**, A970 (1964).

[18]*Handbook of Chemistry and Physics*, 48th ed., edited by R. C. Weast (Chemical Rubber, Cleveland, Ohio, 1967–68), p. D-100.

[19]R. R. Hultgren, R. L. Orr, P. D. Anderson, and K. K. Kelly, *Selected Values of Thermodynamic Properties of Metals and Alloys* (Wiley, New York, 1963), pp. 176, 272, and 308.

[20]T. L. Loucks, Phys. Rev. **143**, 506 (1966).

[21]R. M. Sillitto, *Non-Relativistic Quantum Mechanics* (Quadrangle Books, Chicago, 1960), p. 215.

[22]J. S. Griffith, *The Theory of Transition-Metal Ions* (Cambridge U. P., Cambridge, England, 1961), pp. 52–53.

[23]C. N. Berglund and W. E. Spicer, Phys. Rev. **136**, A1030 (1964).

[24]C. R. Zeisse, in *Proceedings of the Conference on Electronic Density of Electronic Density of States* (Natl. Bur. Std., Gaithersburg, Md., 1969).

[25]K. A. Kress and G. J. Lapeyre, in *Proceedings of Conference on Electronic Density of States* (Natl. Bur. Std., U. S. GPO, Washington, D. C., 1969).